Solitary wave pulses in optical fibers with normal dispersion and higher-order effects

Wen-Jun Liu,[1] Bo Tian,[1,2,3,*] Hai-Qiang Zhang,[1] Tao Xu,[1] and He Li[1,4]

[1]*School of Science, Beijing University of Posts and Telecommunications, P.O. Box 122, Beijing 100876, China*

[2]*State Key Laboratory of Software Development Environment, Beijing University of Aeronautics and Astronautics, Beijing 100191, China*

[3]*Key Laboratory of Information Photonics and Optical Communications, Ministry of Education, Beijing University of Posts and Telecommunications, Beijing 100876, China*

[4]*Ministry-of-Education Key Laboratory of Fluid Mechanics and National Laboratory for Computational Fluid Dynamics, Beijing University of Aeronautics and Astronautics, Beijing 100191, China*

(Received 19 April 2009; revised manuscript received 13 May 2009; published 8 June 2009)

Various types of solitary wave pulses are obtained theoretically based on the analytic solutions for the higher-order nonlinear Schrödinger equation. Different from the previous results, the bright solitons are observed in the normal group-velocity dispersion regime. Depending on the parameters' values, the properties of both bright and dark solitons are analyzed. Furthermore, the soliton types are found to be interchangeable after the collision, and the transfer mode of the solitons can be controlled under certain conditions. This might be of potential applications in the design of optical switch, pulse signal converters, and optical communication systems.

DOI: 10.1103/PhysRevA.79.063810 PACS number(s): 42.65.Tg, 05.45.Yv

I. INTRODUCTION

Optical solitons have been the objects of extensive theoretical and experimental studies in recent years because of their potential applications to telecommunication and ultrafast signal routing systems [1–4]. They evolve from a nonlinear change in the refractive index of a material induced by the light intensity distribution [5]. Although the nonlinear effect is extremely weak, its cumulative effect becomes significant since the communication distance measured by the light wavelength is extremely long [6]. When the combined effects of the group-velocity dispersion (GVD) and the nonlinear change in the refraction index in a fiber exactly compensate each other, the pulse without changes in shape is said to be self-trapped [7]. In the picosecond regime, the main nonlinear equation governing the pulse evolution is the nonlinear Schrödinger (NLS) equation [7], a prototype of the nonlinear evolution equations [2,8,9]. Depending on the sign of the GVD, the NLS equation has two distinct types of localized solutions, bright and dark soliton solutions, which are, respectively, existent in the anomalous and normal dispersion regimes [5].

The existence of the bright solitons in lossless fibers has been theoretically demonstrated [1], and the bright solitons have been experimentally observed [10]. Since then, the propagation of the bright solitons has been verified in a number of well-designed experiments in the anomalous dispersion regime of the fiber spectrum [11]. The applications of various bright solitons can be seen in the aspects of the all-optical switch [12], pulse compression [13], and pulse amplification [14].

In the normal dispersion regime, the existence of the dark solitons was first predicted in Refs. [1,15], experimentally demonstrated in Ref. [16] and confirmed in Ref. [17]. Unlike the bright soliton, a dark soliton appears as an intensity dip in an infinitely extended constant background [18]. It has been investigated in many theoretical and experimental papers, and the early results in this field were summarized in three review papers [5,19,20]. The dark solitons have attracted much attention due to their potential applications [21]. For example, using structures created during the propagation and interaction of the dark solitons, many types of all-optical switches may be written [22]. Other applications of the dark solitons involve the optical logic devices [23] and waveguide optics as dynamic switches and junctions [24]. They are also considered in signal processing and communication because of their inherent stability [25].

Compared with the bright solitons, they have better stability against various perturbations such as fiber loss, mutual interaction between neighboring pulses, the Raman effect, and the superposition of noise emitted from optical amplifiers [26]. However, the results have usually been based on the NLS equation which can describe the soliton behavior applicable to a picosecond regime [27]. For the channel handling large capacity and high speed, it is necessary to transmit solitary waves at a high bit rate of ultrashort pulses [7]. Therefore, it is very important to take into account a number of higher-order effects such as the third-order dispersion (TOD), self-steepening (SS) [28] and the self-frequency shift (SFS) [29] in the propagation of femtosecond pulses. Thus, the NLS equation fails in the physical description of the soliton behavior under these circumstances [27], and the higher-order nonlinear Schrödinger (HNLS) equation [30],

$$i\frac{\partial q}{\partial Z}+\frac{1}{2}\frac{\partial^2 q}{\partial T^2}+|q|^2q+\epsilon i\times\left[\varrho_1+\frac{\partial^3 q}{\partial T^3}+\varrho_2\frac{\partial}{\partial T}(|q|^2q)+\varrho_3 q\frac{\partial}{\partial T}|q|^2\right]=0, \quad (1)$$

has been proposed to describe the soliton behavior in a subpicosecond and femtosecond regimes [31], where q is a complex function and Z and T are the normalized distance and time, respectively. ϵ is a small parameter, ϱ_2 is responsible

*Corresponding author; tian.bupt@yahoo.com.cn

for SS and shock formation, and ϱ_3 is responsible for SFS induced by intrapulse Raman scattering [7,30].

However, we notice that the previous studies have been limited to the dynamics of the bright optical solitons propagating in the anomalous dispersion regime and the dark optical solitons propagating in the normal dispersion regime [1]. In this paper, we consider the theoretical aspects of both bright and dark soliton propagations in the HNLS equation including the higher-order effects such as TOD, SS, and stimulated Raman scattering (SRS). Hirota's method based on the computerized symbolic computation [2,8,9] has made it exercisable to solve the HNLS equation under investigation. In particular, some types of soliton solutions are presented for the HNLS equation under certain parametric conditions.

The structure of the present paper is as follows. In Sec. II, with the aid of symbolic computation, the bilinear form for the HNLS equation is acquired in virtue of Hirota's method. In Sec. III, (A) the one-soliton solution and (B) the two-soliton solution are explicitly presented based on its bilinear form, and the detailed analysis of the solitons via the obtained soliton solutions is performed. Finally, our conclusions are given in Sec. IV.

II. BILINEAR FORM FOR THE HNLS EQUATION

With symbolic computation [2,8,9], in the normal dispersion regime ($\beta_2 > 0$), we present a soliton phenomenon (the bright solitons in the normal dispersion regime) for the HNLS equation. Considering $\alpha L \ll 1$, where L is the fiber length and α is negligible [7], the HNLS equation describing the propagation of femtosecond pulses in optical fibers can be written in the form [30,32]

$$\frac{\partial u}{\partial \xi} + \frac{i}{2}\frac{\partial^2 u}{\partial \tau^2} + \frac{1}{6}L\frac{\partial^3 u}{\partial \tau^3} - iN^2|u|^2u + sN^2\frac{\partial}{\partial \tau}(|u|^2u) - \tau_R N^2 u\frac{\partial |u|^2}{\partial \tau} = 0, \tag{2}$$

where u is the normalized amplitude, ξ represents the normalized propagation distance, τ is the normalized time, and

$$L = \frac{L_D}{L_D'}, \quad L_D = \frac{T_0^2}{|\beta_2|}, \quad L_D' = \frac{T_0^3}{|\beta_3|}, \quad N^2 = \frac{L_D}{L_{NL}},$$

$$L_{NL} = \frac{1}{\gamma P_0}, \quad s = \frac{1}{\omega_0 T_0}, \quad \tau_R = \frac{T_R}{T_0}, \tag{3}$$

in which, L_D is the dispersion length, L_D' is a dispersion length associated with the TOD, and T_0 is the half width (at $1/e$ intensity point) of the input pulse. In practice, it is customary to use the full width at half maximum (FWHM) in place of T_0. For a hyperbolic-secant pulse, the two variables are related as $T_{FWHM} = 2\ln(1+\sqrt{2})T_0 \approx 1.763T_0$. β_2 represents the GVD parameter, β_3 is the TOD coefficient, N is the soliton order, L_{NL} is the nonlinear length, γ is the fiber nonlinearity coefficient in units of $W^{-1}\,km^{-1}$, P_0 is the peak power of the incident pulse, and ω_0 is the carrier frequency. The parameters s and τ_R account for, respectively, the effects of SS and SRS.

By introducing the dependent variable transformation [33]

$$u = \frac{g(\xi,\tau)}{f(\xi,\tau)}, \tag{4}$$

where $g(\xi,\tau)$ is a complex differentiable function and $f(\xi,\tau)$ is a real one, after some symbolic manipulations, the bilinear form for Eq. (2) is obtained as

$$\left(D_\xi + \frac{i}{2}D_\tau^2 + \frac{1}{6}LD_\tau^3 + \lambda\right)gf = 0, \tag{5}$$

$$(D_\tau^2 - 2i\lambda)ff = -2N^2|g|^2. \tag{6}$$

The constraint of the coefficients is $s = L = \tau_R/2$. Here, λ is a constant to be determined and Hirota's bilinear operators D_ξ and D_τ [34] are defined by

$$D_\xi^m D_\tau^n (a\cdot b) = \left(\frac{\partial}{\partial \xi} - \frac{\partial}{\partial \xi'}\right)^m \times \left(\frac{\partial}{\partial \tau} - \frac{\partial}{\partial \tau'}\right)^n a(\xi,\tau)b(\xi',\tau')|_{\xi'=\xi,\tau'=\tau}. \tag{7}$$

Equations (5) and (6) can be solved by introducing the following power series expansions for g and f:

$$g = g_0(1 + \varepsilon g_1 + \varepsilon^2 g_2 + \cdots), \tag{8}$$

$$f = 1 + \varepsilon f_1 + \varepsilon^2 f_2 + \cdots, \tag{9}$$

where ε is a formal expansion parameter and $f_1, f_2, \ldots, g_1, g_2, \ldots$ are assumed to go to zero as $\xi \to -\infty$. Substituting Eqs. (8) and (9) into Eqs. (5) and (6) and equating coefficients of the same powers of ε to zero can yield the recursion relations for $f_n(\xi,\tau)$ and $g_n(\xi,\tau)$ $(n = 1,2,\ldots)$.

III. SOLITON SOLUTIONS FOR THE HNLS EQUATION

The bilinear form for Eq. (2) is presented in the above section with the coefficient constraint. Next, the soliton solutions will be obtained, and the effects of the parameters in the model will be discussed.

A. One-soliton solution

To obtain the dark one-soliton solution for Eq. (2), we assume that

$$g_0 = \mu e^\theta, \quad g_1 = -e^\vartheta, \quad f_1 = \beta e^\vartheta, \tag{10}$$

where μ is an arbitrary complex parameter, $\theta = ia\xi + ib\tau$ with a, b as real constants, and $\vartheta = k\xi + \omega\tau + \delta$ with k, ω as arbitrary complex parameters and δ and β as real constants. Substituting $g(\xi,\tau)$ into the resulting set of linear partial differential equations, we can get

$$a = \frac{1}{6}(Lb^3 + 3b^2 - 6N^2 s\mu\mu^* b + 6N^2\mu\mu^*),$$

$$k = \frac{1}{6}(-L\omega^3 + 6b\omega + 3b^2 L\omega - 18N^2 s\mu\mu^*\omega + 12N^2\mu\mu^*\tau_R\omega),$$

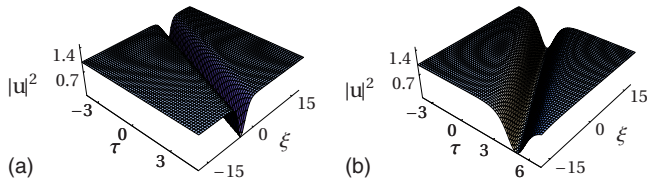

FIG. 1. (Color online) Intensity profile of the dark soliton solution expressed via solution (11). The parameters adopted here are $N=1$, $\mu=i$, $\delta=4$ with (a) $s=2$, $\tau_R=4$, $L=2$, (b) $s=0.5$, $\tau_R=1$, and $L=0.5$.

$$\omega^2 = \frac{4(N^2\mu\mu^* - bN^2 s\mu\mu^*)}{1+bL},$$

$$b = \frac{-L-3s+2\tau_R}{2L(s-\tau_R)}, \quad \beta = 1, \quad \lambda = -iN^2\mu\mu^*,$$

and

$$g_n(\xi,\tau) = 0, \quad f_n(\xi,\tau) = 0 \quad (n = 2,3,4,\ldots).$$

Here, the asterisk denotes the complex conjugate. Without loss of generality, we set $\varepsilon=1$. Thus, the one-soliton solution can be explicitly expressed as

$$u = \frac{g}{f} = \frac{g_0(1+g_1)}{1+f_1} = \frac{\mu e^{\theta}(1-e^{\vartheta})}{1+e^{\vartheta}} = \mu e^{\theta}\tanh\left(-\frac{\vartheta}{2}\right). \tag{11}$$

According to Eq. (11), the dark soliton propagating in the normal dispersion regime is presented in Fig. 1.

Figure 1 shows that the dark soliton is remarkably stable during the propagation. The effects of GVD can be counterbalanced perfectly by the nonlinear effects without changing in shape. If the effects of TOD, SS, and SRS are changed in the above circumstance, the propagation speed of the soliton will be influenced. When the effects of TOD, SS, and SRS are enhanced in Fig. 1(a), the soliton speed becomes faster correspondingly. Because the effects of TOD, SS, and SRS are associated with the pulse power, the greater the pulse power is, the more obvious the nonlinear effects will be. Moreover, the pulse speed increases accompanied by an increase in the pulse energy. Hence, by increasing the value of s, τ_R and L, the pulse speed can become faster. In Fig. 1(b), the conclusion that we have derived from Fig. 1(a) is further conformed. In fact, the pulse speed in Fig. 1 can be expressed as $v=3/(2L\mu\mu^*+9s\mu\mu^*-6\tau_R\mu\mu^*)$. Thus, the speed

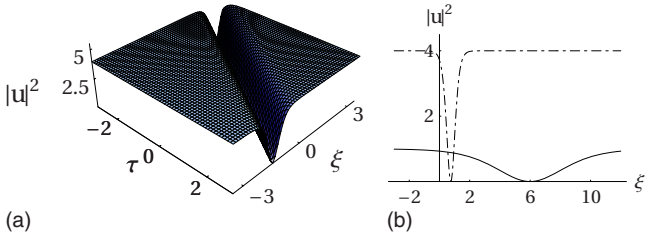

FIG. 2. (Color online) Intensity profile of the dark soliton solution expressed via solution (11). The parameters adopted here are $N=1$, $s=1$, $\tau_R=2$, $L=1$, $\delta=4$, and $\mu=2i$: (a) temporal evolution for the dark soliton and (b) comparison between $\mu=i$ (in the solid curve) and $\mu=2i$ (in the dashed curve).

of the pulse is related to s, L, τ_R and μ. In the next part, we will change the value of μ and discuss its influence.

Compared with Fig. 1, the value of μ is replaced by $2i$ in Fig. 2(a). Not only dose the speed of the pulse increase, but also the intensity of the pulse is enhanced. This phenomenon can be explained by solution (11). The pulse intensity is proportional to μ. On the contrary, the pulse intensity and the pulse speed will decrease if the value of μ is reduced. Among the parameters in solution (11), the effects of s, L, τ_R and μ are discussed. When changing the value of δ in solution (11), the pulse will go through the phase shift. There is a right shift of the phase when the value of δ is increased, while the left shift appears when δ is decreased. From solution (11), we can find that the pulse phase is equal to $-\delta/2$. Thus, the pulse phase is determined by δ.

B. Two-soliton solution

In the following, in order to find the two-soliton solution, we can assume

$$g_0 = \mu e^{\psi},$$

$$g_1 = (\gamma_1 + i\delta_1)e^{\psi_1} + (\gamma_2 + i\delta_2)e^{\psi_2},$$

$$g_2 = A(\gamma_1 + i\delta_1)(\gamma_2 + i\delta_2)e^{\psi_1+\psi_2},$$

$$f_1 = B_1 e^{\psi_1} + B_2 e^{\psi_2}, \quad f_2 = Be^{\psi_1+\psi_2}, \tag{12}$$

where $\psi=i\eta\xi$, $\psi_j=k_j\xi+\omega_j\tau (j=1,2)$ with η, k_j, and ω_j as real constants, B_j is an arbitrary real constant, and γ_j, δ_j, A and B are all complex parameters to be determined. Then, by solving the resulting linear partial differential equations recursively, we can write the two-soliton solution explicitly as

$$u = \frac{g}{f} = \frac{g_0(1+g_1+g_2)}{1+f_1+f_2} = \mu e^{\psi}\frac{1+(\gamma_1+i\delta_1)e^{\psi_1}+(\gamma_2+i\delta_2)e^{\psi_2}+A(\gamma_1+i\delta_1)(\gamma_2+i\delta_2)e^{\psi_1+\psi_2}}{1+B_1e^{\psi_1}+B_2e^{\psi_2}+Be^{\psi_1+\psi_2}}, \tag{13}$$

where

$$\gamma_j = B_j\cos(\Omega_j), \quad \delta_j = B_j\sin(\Omega_j), \quad \eta = N^2\mu\mu^*, \quad \omega_j^2 = 2[1-\cos(\Omega_j)]N^2\mu\mu^*,$$

$$k_j = -\frac{1}{6}\omega_j^2\left[3\cot\left(\frac{\Omega_j}{2}\right) + L\omega_j\right],$$

$$A = \frac{C - 2\cos\left(\frac{\Omega_1-\Omega_2}{2}\right)\omega_2\omega_1 - L\sin\left(\frac{\Omega_1-\Omega_2}{2}\right)\omega_2(\omega_1-\omega_2)\omega_1}{C - 2\cos\left(\frac{\Omega_1+\Omega_2}{2}\right)\omega_2\omega_1 - L\sin\left(\frac{\Omega_1+\Omega_2}{2}\right)\omega_2(\omega_1+\omega_2)\omega_1},$$

$$B = B_1B_2\frac{C - 2\cos\left(\frac{\Omega_1-\Omega_2}{2}\right)\omega_2\omega_1 - L\sin\left(\frac{\Omega_1-\Omega_2}{2}\right)\omega_2(\omega_1-\omega_2)\omega_1}{C - 2\cos\left(\frac{\Omega_1+\Omega_2}{2}\right)\omega_2\omega_1 - L\sin\left(\frac{\Omega_1+\Omega_2}{2}\right)\omega_2(\omega_1+\omega_2)\omega_1},$$

$$C = \csc\left(\frac{\Omega_1}{2}\right)\sin\left(\frac{\Omega_2}{2}\right)\omega_1^2 + \csc\left(\frac{\Omega_2}{2}\right)\sin\left(\frac{\Omega_1}{2}\right)\omega_2^2,$$

$$g_n(\xi,\tau) = 0, \quad f_n(\xi,\tau) = 0 \quad (n = 3,4,5,\ldots), \tag{14}$$

with Ω_j as arbitrary angles.

1. $B_1 = B_2 = 1$

Solution (13) is the usual two-soliton solution shown in Fig. 3(a). We can get the dark solitons when the values of B_1 and B_2 are both positive. The two dark solitons interact with each other and propagate stably before and after collision. In Fig. 3(a), the two pulses are incidented with an angle when $\Omega_1 = \pi/2$ and $\Omega_2 = -\pi/2$. As long as Ω_1 and Ω_2 have the opposite sign, the solitons expressed by solution (13) will always have the two dark solitons properties. However, if Ω_1 and Ω_2 have the same sign, they will show different intriguing characteristics owing to the different choices of ω_1 and ω_2.

(i) $|\omega_1| = |\omega_2|$. When $\Omega_1 = \Omega_2 = -\pi/2$ and $\omega_1 = \omega_2 = 2\sqrt{2}$, the two dark solitons degenerate into the fundamental soliton shown in Fig. 3(b). The two solitons have the exactly same parameters, so Fig. 3(a) turns into Fig. 3(b). If ω_1 and ω_2 have the opposite signs, the solitons show an interesting phenomenon. The transfer mode of the two dark solitons evolves into the one-way transfer mode in Fig. 4. It is strange that the propagation directions of the two pulses are different when they spread to both sides of ξ. Their dissemination determined by the values of Ω_1 and Ω_2 is only in one direction and has been accompanied by a certain angle, but they will never intersect with each other. To our knowledge, this phenomenon has not been reported in previous studies. We hope this result will be valuable to the design of optical switch and optical communication systems.

(ii) $|\omega_1| < |\omega_2|$. The above analysis is based on the condition that $|\omega_1| = |\omega_2|$. In this case, we will discuss the changes when $|\omega_1| < |\omega_2|$. Compared with Fig. 3(a), there are only angle changes between the incident pulses on the condition that $\Omega_1\Omega_2 < 0$. When $\Omega_1\Omega_2 > 0$, the soliton type is determined by the value of ω_2. If ω_2 is negative, we can also get the two dark solitons which are in parallel as shown in Fig. 5. Interestingly, they do not interact with each other even if they are overlapped with each other during the propagation. This might be a potential application in communication systems which can enhance the capacity of the systems.

In contrast, when ω_2 is positive, the bright solitons are observed in Fig. 6 no matter the value of ω_1 is positive or negative. This result is very surprising as it is well known

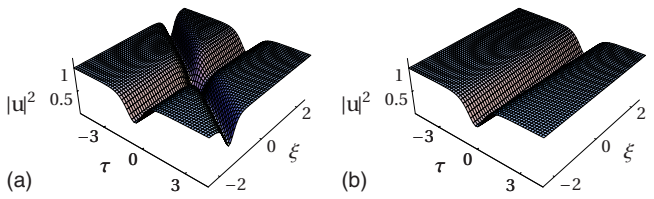

FIG. 3. (Color online) Intensity profiles of the two-soliton solution expressed via solution (13). The parameters adopted here are as follows: $B_1 = B_2 = 1$, $N = 2$, $L = 1$, $\mu = i$, and $\omega_1 = \omega_2 = 2\sqrt{2}$ with (a) $\Omega_1 = \pi/2$, $\Omega_2 = -\pi/2$ and (b) $\Omega_1 = \Omega_2 = -\pi/2$.

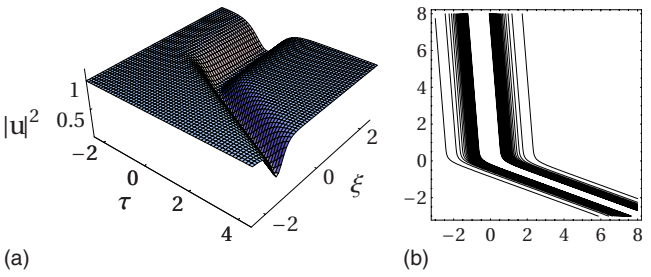

FIG. 4. (Color online) Intensity profiles of the two-soliton solution expressed via solution (13). The parameters adopted here are as follows: $B_1 = B_2 = 1$, $N = 2$, $L = 1$, $\mu = i$, $\omega_1 = 2\sqrt{2}$, and $\omega_2 = -2\sqrt{2}$ with (a) $\Omega_1 = \pi/2$, $\Omega_2 = \pi/2$ and (b) the contour plot of (a).

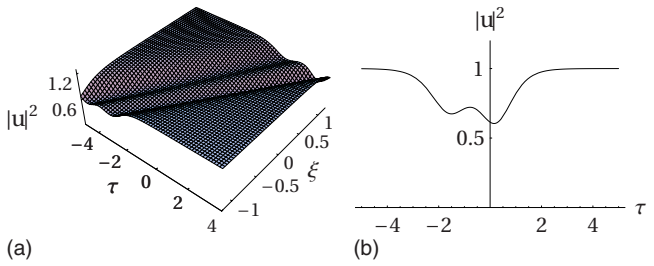

FIG. 5. (Color online) Intensity profiles of the two-soliton solution expressed via solution (13). The parameters adopted here are as follows: (a) $B_1=B_2=1$, $N=2$, $L=1$, $\mu=i$, $\Omega_1=-\pi/3$, $\Omega_2=-\pi/2$, $\omega_1=-2$, $\omega_2=-2\sqrt{2}$ and (b) the cross section plot of (a).

that the bright solitons cannot propagate in the normal GVD regime. From Fig. 6(b), we can find that the solitons interact with each other. Moreover, they can propagate without interaction if the incidence angle is chosen appropriately.

It is important to note that the solitons exchange their energy and types during the collision. Figure 6(b) shows that the solitons have a phase shift after collision. However, unlike those previously observed, the bright soliton (before collision) is transformed into the dark one (after collision), and the dark soliton (before collision) is changed into the bright one (after collision). In order to understand the collision in a more explicit manner, we analyze the asymptotic limits of two-soliton solution (13) as follows:

(1) Before collision ($\xi\to-\infty$),

$$\text{(a)}\quad \psi_1+\psi_1^*\sim 0,\quad \psi_2+\psi_2^*\to-\infty:$$

$$u_1^-\to\frac{\mu e^{\psi}[1+(\gamma_1+i\delta_1)e^{\psi_1}]}{1+B_1e^{\psi_1}},\tag{15}$$

$$\text{(b)}\quad \psi_2+\psi_2^*\sim 0,\quad \psi_1+\psi_1^*\to+\infty:$$

$$u_2^-\to\frac{\mu e^{\psi}(\gamma_1+i\delta_1)[1+(\gamma_2+i\delta_2)Ae^{\psi_2}]}{B_1+Be^{\psi_2}}.\tag{16}$$

(2) After collision ($\xi\to+\infty$),

$$\text{(a)}\quad \psi_1+\psi_1^*\sim 0,\quad \psi_2+\psi_2^*\to+\infty:$$

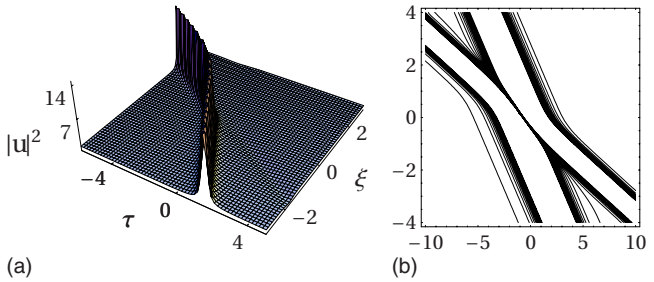

FIG. 6. (Color online) Intensity profiles of the two-soliton solution expressed via solution (13). The parameters adopted here are as follows: $B_1=B_2=1$, $N=2$, $L=1$, and $\mu=i$ with (a) $\Omega_1=\pi/3$, $\Omega_2=\pi/2$, $\omega_1=-2$, $\omega_2=2\sqrt{2}$ and (b) the contour plot of (a).

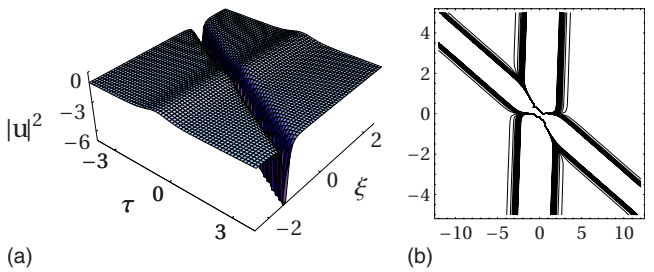

FIG. 7. (Color online) Intensity profiles of the two-soliton solution expressed via solution (13). The parameters adopted here are as follows: (a) $B_1=1$, $B_2=-1$, $\omega_1=2\sqrt{2}$, $\omega_2=2\sqrt{2}$, $\Omega_1=-\pi/2$, $\Omega_2=\pi/2$ and (b) the contour plot of (a).

$$u_1^+\to\frac{\mu e^{\psi}(\gamma_2+i\delta_2)[1+(\gamma_1+i\delta_1)Ae^{\psi_1}]}{B_2+Be^{\psi_1}},\tag{17}$$

$$\text{(b)}\quad \psi_2+\psi_2^*\sim 0,\quad \psi_1+\psi_1^*\to-\infty:$$

$$u_2^+\to\frac{\mu e^{\psi}[1+(\gamma_2+i\delta_2)e^{\psi_2}]}{1+B_2e^{\psi_2}}.\tag{18}$$

According to the above expressions, it has been proved that the total energy of the solitons is conserved before and after collision, that is,

$$|u_1^-|^2+|u_2^-|^2=|u_1^+|^2+|u_2^+|^2.\tag{19}$$

Furthermore, u_1^- and u_2^+ have the same soliton type and so do u_1^+ and u_2^-. Therefore, the soliton type is interchanged during the collision. This result might have potential applications in the study of pulse signal converters.

(iii) $|\omega_1|>|\omega_2|$. In this case, the two dark solitons can be obtained when $\Omega_1\Omega_2<0$ which is similar to the above section. But the soliton type is determined by ω_1 instead of ω_2 if $\Omega_1\Omega_2>0$. When ω_1 is positive, the two dark solitons [such as Fig. 3(a)] can be observed. Figure 6 can also be obtained if ω_1 is chosen to be negative.

Subsequently, we mainly focus on the phenomena when B_1 and B_2 are given in other cases: (1) $B_1B_2<0$; (2) $B_1<0$ and $B_2<0$. By virtue of solution (13), the different combinations of B_1, B_2, Ω_1, Ω_2, ω_1, and ω_2 are investigated, with the corresponding parameters chosen as $N=2$, $\mu=i$, and $L=1$.

2. $B_1=\pm B_2$ and $B_1=\pm 1$

(i) $|\omega_1|=|\omega_2|$. Under the above precondition, the dark and bright solitons are presented in Fig. 7 when $\Omega_1\Omega_2<0$. The collision between the solitons is elastic, and there is only the shift of the soliton phase. If $\Omega_1\Omega_2>0$ and $\omega_1=\omega_2$, solution (13) evolves into a constant. Otherwise, if $\Omega_1\Omega_2>0$ and $\omega_1=-\omega_2$, other types of peculiar phenomena will appear.

Similar to Fig. 4, the transfer mode of the bright and dark solitons evolves into the one-way transfer mode. Interchanging the signs of ω_1 and ω_2, we can control the soliton types along the direction of ξ. Correspondingly, the soliton propagation direction can also be controlled by changing the signs of Ω_1 and Ω_2.

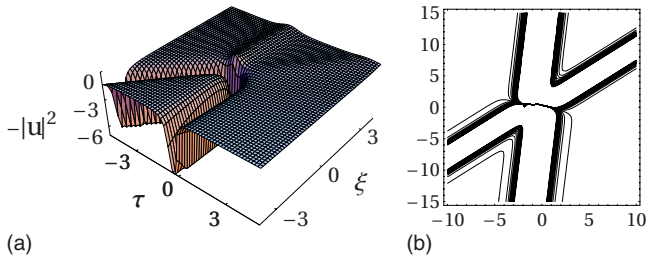

FIG. 8. (Color online) Intensity profiles of the two-soliton solution expressed via solution (13). The parameters adopted here are as follows: $B_1=1$, $B_2=1$ with (a) $\Omega_1=-\pi/3$, $\Omega_2=-\pi/2$, $\omega_1=2$, $\omega_2=2\sqrt{2}$ and (b) the contour plot of (a).

(ii) $|\omega_1|<|\omega_2|$. In this section, the dark and bright solitons can also be obtained (such as Fig. 7) in two cases: (1) $\Omega_1\Omega_2<0$; (2) $\Omega_1\Omega_2>0$ and $\omega_2<0$. If $\Omega_1\Omega_2>0$ and $\omega_2>0$, the similar situation in Fig. 6 appears again in Fig. 8. The bright and dark solitons interchange their soliton types and energy after collision.

(iii) $|\omega_1|>|\omega_2|$. This case is the same as $|\omega_1|<|\omega_2|$ when $\Omega_1\Omega_2<0$. If $\Omega_1\Omega_2>0$, the soliton collision situation is mainly determined by ω_1. When $\omega_1<0$, we can get the elastic collision phenomena shown in Fig. 7. On the contrary, when $\omega_1>0$, the similar situation is presented in Fig. 9. Although the incidence angle and direction are different owing to the different values of ω_1, ω_2, Ω_1, and Ω_2, the soliton collision is quite similar to Fig. 8 essentially.

3. $B_1=B_2=-1$

(i) $|\omega_1|=|\omega_2|$. If the signs of B_1 and B_2 are both negative and $\Omega_1\Omega_2<0$, the bright two solitons can be observed in the normal GVD regime. There is a large phase shift between them after collision. The two bright solitons are both stable before and after collision in the normal regime. If $\Omega_1\Omega_2>0$ and $\omega_1=\omega_2$, the two bright solitons can be simplified as the fundamental bright soliton. This case is similar to Fig. 3(b). Because $\psi_1=\psi_2$ in expression (12), solution (13) has the same form with solution (11). If $\Omega_1\Omega_2>0$ and $\omega_1=-\omega_2$, the transfer mode of the bright solitons is also changed, shown in Fig. 10. Through changing the signs of Ω_1, Ω_2, ω_1, and ω_2, the propagation direction can be controlled.

(ii) $|\omega_1|<|\omega_2|$. We can get the two bright solitons under both of the following conditions: (1) $\Omega_1\Omega_2<0$; (2) $\Omega_1\Omega_2>0$ and $\omega_2<0$. The two conditions are similar to those when $B_1=\pm B_2$. What is different is that the two bright solitons are obtained in this case while the bright and dark solitons are

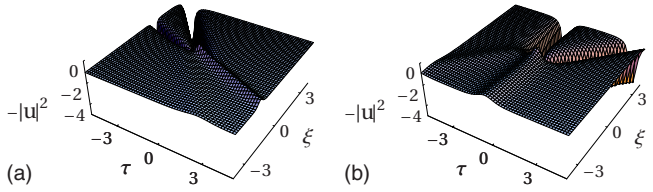

FIG. 9. (Color online) Intensity profiles of the two-soliton solution expressed via solution (13). The parameters adopted here are as follows: $B_1=1$ and $B_2=-1$ with (a) $\Omega_1=\pi/2$, $\Omega_2=\pi/3$, $\omega_1=2\sqrt{2}$, $\omega_2=-2$ and (b) $\Omega_1=-\pi/2$, $\Omega_2=-\pi/3$, $\omega_1=2\sqrt{2}$, $\omega_2=2$.

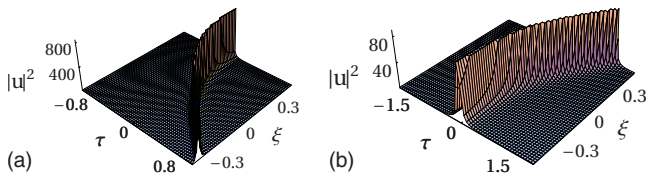

FIG. 10. (Color online) Intensity profiles of the two-soliton solution expressed via solution (13). The parameters adopted here are as follows: $B_1=-1$ and $B_2=-1$ with (a) $\Omega_1=\pi/2$, $\Omega_2=\pi/2$, $\omega_1=2\sqrt{2}$, $\omega_2=-2\sqrt{2}$ and (b) $\Omega_1=-\pi/2$, $\Omega_2=-\pi/2$, $\omega_1=-2\sqrt{2}$, $\omega_2=2\sqrt{2}$.

observed in another case. When $\Omega_1\Omega_2>0$ and $\omega_2>0$, further validation of the peculiar changes of the soliton types are presented in Fig. 11. Similar to Fig. 6, the solitons undergo the conversion of the soliton types.

(iii) $|\omega_1|>|\omega_2|$. The two bright solitons can also be observed in the following two cases: (1) $\Omega_1\Omega_2<0$; (2) $\Omega_1\Omega_2>0$ and $\omega_1<0$. The only difference with $|\omega_1|<|\omega_2|$ is that ω_2 is replaced by ω_1. Correspondingly, the phenomena in Fig. 11 appear again when $\omega_1>0$.

IV. CONCLUSIONS

In conclusion, we have investigated the HNLS equation, which can be used to describe the solitons propagating in the subpicosecond or femtosecond regime. With the aid of symbolic computation, we have carried out our study from an analytical viewpoint. By directly applying Hirota's method, the analytic one- and two-soliton solutions of this model have been obtained. Of physical and optical interests, relevant properties of the solitons have been analyzed and graphically discussed in details depending on the parameters' values (192 kinds of combinations in total). Among them, the bright solitons have been observed in the normal GVD regime. In addition, an interesting phenomenon has been found that the transfer mode of the two solitons can evolve into the one-way transfer mode during the propagation. Moreover, through an asymptotic analysis for the two-soliton solution, we have found that the soliton types can be interchanged after collision. Attention should be emphasized as below:

(1) In the normal GVD regime, the bright and dark solitons have both been displayed by changing the values of the parameters. This conclusion may provide a reference for the

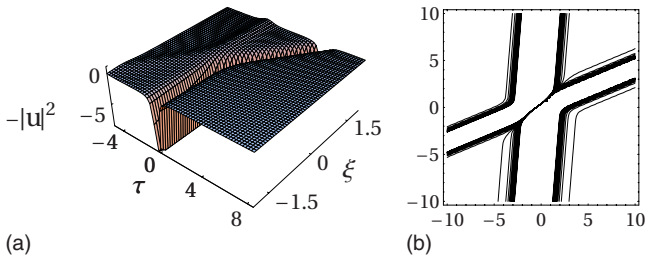

FIG. 11. (Color online) Intensity profiles of the two-soliton solution expressed via Solution (13). The parameters adopted here are as follows: (a) $B_1=-1$, $B_2=-1$, $\Omega_1=-\pi/3$, $\Omega_2=-\pi/2$, $\omega_1=-2$, $\omega_2=2\sqrt{2}$, and (b) the contour plot of (a).

optical communication system design which is expected to produce the bright and dark solitons simultaneously.

(2) It is worth noting that, to our knowledge, the conversion of the soliton transfer mode has almost not been reported. This result can be used in the design of optical switch and optical communication systems. This is why we are interested in the study and the ultimate goal of our research.

(3) After collision, the solitons can alter their types, which is promising in the potential applications in the design of pulse signal converters and high-speed optical devices in ultralarge capacity transmission systems. This means that we are able to control the soliton types with suitably selected values of the parameters. We expect that the above phenomena could be observed in the experiments.

The obtained results are of certain applications in controlling the information sequences of ultrashort pulses in fiber communications lines through controlling the incidence angle between the solitons. We believe that those results will be useful for the future study in optical communications.

ACKNOWLEDGMENTS

We express our sincere thanks to a referee and Professor Y. T. Gao for their valuable comments. This work was supported by the National Natural Science Foundation of China under Grant No. 60772023, by the Open Fund of the State Key Laboratory of Software Development Environment under Grant No. SKLSDE-07-001, Beijing University of Aeronautics and Astronautics, by the National Basic Research Program of China (973 Program) under Grant No. 2005CB321901, and by the Specialized Research Fund for the Doctoral Program of Higher Education (Grants No. 20060006024 and No. 200800130006), Chinese Ministry of Education.

[1] A. Hasegawa and F. Tappert, Appl. Phys. Lett. **23**, 142 (1973); **23**, 171 (1973).

[2] B. Tian, W. R. Shan, C. Y. Zhang, G. M. Wei, and Y. T. Gao, Eur. Phys. J. B **47**, 329 (2005); B. Tian and Y. T. Gao, Phys. Lett. A **342**, 228 (2005); **359**, 241 (2006); B. Tian, Y. T. Gao, and H. W. Zhu, *ibid.* **366**, 223 (2007); W. J. Liu, B. Tian, H. Q. Zhang, L. L. Li, and Y. S. Xue, Phys. Rev. E **77**, 066605 (2008).

[3] Z. H. Li, L. Li, H. P. Tian, G. S. Zhou, and K. H. Spatschek, Phys. Rev. Lett. **89**, 263901 (2002); Z. Y. Xu, L. Li, Z. H. Li, G. S. Zhou, and K. Nakkeeran, Phys. Rev. E **68**, 046605 (2003); R. Y. Hao, L. Li, Z. H. Li, and G. S. Zhou, *ibid.* **70**, 066603 (2004); R. C. Yang, L. Li, R. Y. Hao, Z. H. Li, and G. S. Zhou, *ibid.* **71**, 036616 (2005).

[4] M. Vijayajayanthi, T. Kanna, and M. Lakshmanan, Phys. Rev. A **77**, 013820 (2008).

[5] Y. S. Kivshar and B. Luther-Davies, Phys. Rep. **298**, 81 (1998).

[6] A. Hasegawa, Chaos **10**, 475 (2000).

[7] G. P. Agrawal, *Nonlinear Fiber Optics*, 3rd ed. (Academic, California, 2002).

[8] M. P. Barnett, J. F. Capitani, J. Von Zur Gathen, and J. Gerhard, Int. J. Quantum Chem. **100**, 80 (2004); Z. Y. Yan and H. Q. Zhang, J. Phys. A **34**, 1785 (2001); B. Tian and Y. T. Gao, Phys. Lett. A **340**, 243 (2005); **362**, 283 (2007); B. Tian, H. Li, and Y. T. Gao, ZAMP **56**, 783 (2005); W. J. Liu, B. Tian, and H. Q. Zhang, Phys. Rev. E **78**, 066613 (2008).

[9] G. Das and J. Sarma, Phys. Plasmas **6**, 4394 (1999); W. P. Hong, Phys. Lett. A **361**, 520 (2007); B. Tian and Y. T. Gao, Phys. Plasmas **12**, 070703 (2005); Eur. Phys. J. D **33**, 59 (2005); Y. T. Gao and B. Tian, Phys. Lett. A **349**, 314 (2006); **361**, 523 (2007); Phys. Plasmas **13**, 112901 (2006); **13**, 120703 (2006); EPL **77**, 15001 (2007); W. J. Liu, X. H. Meng, K. J. Cai, X. Lü, T. Xu, and B. Tian, J. Mod. Opt. **55**, 1331 (2008).

[10] L. F. Mollenauer, R. H. Stolen, and J. P. Gordon, Phys. Rev. Lett. **45**, 1095 (1980).

[11] S. A. Ponomarenko, N. M. Litchinitser, and G. P. Agrawal, Phys. Rev. E **70**, 015603(R) (2004); D. E. Pelinovsky, P. G. Kevrekidis, D. J. Frantzeskakis, and V. Zharnitsky, *ibid.* **70**, 047604 (2004).

[12] R. A. Vicencio, M. I. Molina, and Y. S. Kivshar, Phys. Rev. E **71**, 056613 (2005); R. Radhakrishnan and M. Lakshmanan, *ibid.* **60**, 2317 (1999); J. K. Yang, *ibid.* **59**, 2393 (1999); R. Radhakrishnan, M. Lakshmanan, and J. Hietarinta, *ibid.* **56**, 2213 (1997); W. C. K. Mak, B. A. Malomed, and P. L. Chu, *ibid.* **55**, 6134 (1997); R. Gomez-Alcala and A. Dengra, Opt. Lett. **31**, 3137 (2006).

[13] K. Senthilnathan, Q. Li, K. Nakkeeran, and P. K. A. Wai, Phys. Rev. A **78**, 033835 (2008); L. Y. Wang, L. Li, Z. H. Li, G. S. Zhou, and D. Mihalache, Phys. Rev. E **72**, 036614 (2005).

[14] R. A. Vicencio, M. I. Molina, and Y. S. Kivshar, Opt. Lett. **29**, 2905 (2004); S. A. Ponomarenko and G. P. Agrawal, Phys. Rev. Lett. **97**, 013901 (2006).

[15] V. E. Zakharov and A. B. Shabat, Zh. Eksp. Teor. Fiz. **64**, 1627 (1973) [Sov. Phys. JETP **37**, 823 (1973)].

[16] P. Emplit, J. P. Hamaide, F. Reynaud, C. Froehly, and A. Barthélémy, Opt. Commun. **62**, 374 (1987).

[17] A. M. Weiner, J. P. Heritage, R. J. Hawkins, R. N. Thurston, E. M. Kirschner, D. E. Leaird, and W. J. Tomlinson, Phys. Rev. Lett. **61**, 2445 (1988).

[18] W. Królikowski, N. Akhmediev, and B. Luther-Davies, Phys. Rev. E **48**, 3980 (1993).

[19] A. M. Weiner, *Optical Solitons: Theory and Experiment* (Cambridge University, Cambridge, England, 1992).

[20] Y. S. Kivshar, IEEE J. Quantum Electron. **29**, 250 (1993).

[21] A. Ciattoni, B. Crosignani, S. Mookherjea, and A. Yariv, Opt. Lett. **30**, 516 (2005); G. R. Lin, C. L. Pan, and I. H. Chiu, *ibid.* **31**, 835 (2006); N. Q. Ngo, *ibid.* **32**, 3402 (2007); A. Dreischuh, D. N. Neshev, D. E. Petersen, O. Bang, and W. Krolikowski, Phys. Rev. Lett. **96**, 043901 (2006); A. M. Kamchatnov and L. P. Pitaevskii, *ibid.* **100**, 160402 (2008); W. X. Yang, J. M. Hou, and R. K. Lee, Phys. Rev. A **77**, 033838 (2008); X. F. Zhang, Q. Yang, J. F. Zhang, X. Z. Chen, and W. M. Liu, *ibid.* **77**, 023613 (2008).

[22] B. Luther-Davies and X. P. Yang, Opt. Lett. **17**, 1755 (1992).

[23] G. A. Swartzlander, Jr., Opt. Lett. **17**, 493 (1992).
[24] B. Luther-Davies and X. P. Yang, Opt. Lett. **17**, 496 (1992).
[25] D. Krökel, N. J. Halas, G. Giuliani, and D. Grischkowsky, Phys. Rev. Lett. **60**, 29 (1988).
[26] W. Zhao and E. Bourkoff, Opt. Lett. **14**, 703 (1989); M. Lisak, D. Anderson, and B. A. Malomed, *ibid.* **16**, 1936 (1991); W. Zhao and E. Bourkoff, *ibid.* **14**, 1371 (1989); I. M. Uzunov and V. S. Gerdjikov, Phys. Rev. A **47**, 1582 (1993); J. P. Hamaide, P. Emplit, and M. Haelterman, Opt. Lett. **16**, 1578 (1991); Y. S. Kivshar, M. Haelterman, P. Emplit, and J. P. Hamaide, *ibid.* **19**, 19 (1994).
[27] S. H. Chen, D. F. Shi, and L. Yi, Phys. Rev. E **69**, 046602 (2004).
[28] D. Anderson and M. Lisak, Phys. Rev. A **27**, 1393 (1983).
[29] F. M. Mitschke and L. F. Mollenauer, Opt. Lett. **11**, 659 (1986); J. P. Gordon, *ibid.* **11**, 662 (1986).
[30] Y. Kodama and A. Hasegawa, IEEE J. Quantum Electron. **23**, 510 (1987).
[31] D. Mihalache, N. Truta, and L. C. Crasovan, Phys. Rev. E **56**, 1064 (1997); M. Gedalin, T. C. Scott, and Y. B. Band, Phys. Rev. Lett. **78**, 448 (1997); K. Porsezian and K. Nakkeeran, *ibid.* **76**, 3955 (1996); **74**, 2941 (1995); Z. H. Li, L. Li, H. P. Tian, and G. S. Zhou, *ibid.* **84**, 4096 (2000).
[32] Y. Kodama, J. Stat. Phys. **39**, 597 (1985).
[33] R. Hirota, J. Math. Phys. **14**, 805 (1973).
[34] R. Hirota, Phys. Rev. Lett. **27**, 1192 (1971); J. J. C. Nimmo and N. C. Freeman, J. Phys. A **17**, 1415 (1984).